CrossMark

ORIGINAL ARTICLE

Statistical analysis of the 2003–2016 seismicity of Azerbaijan and surrounding areas

**Luciano Telesca · Fakhraddin Kadirov ·
Gurban Yetirmishli · Rafig Safarov · Gulam Babayev ·
Saida Ismaylova**

Abstract The aim of the present work is to furnish a detailed picture of the space-time-magnitude statistical properties of the instrumental seismic catalogue of Azerbaijan and surrounding regions from 2003 to 2016. Although Azerbaijan is one of the most seismically active areas in the world, an exhaustive description of the statistical properties of the time, space, and magnitude distribution of its seismicity is still lacking. Therefore, the aim of this work is to fill this scientific gap.

1 Introduction

The territory of Azerbaijan is located within the central part of the Mediterranean tectonic belt, whose seismicity

L. Telesca (✉)
National Research Council, Institute of Methodologies for Environmental Analysis, C.da S. Loja, 85050 Tito, PZ, Italy
e-mail: luciano.telesca@imaa.cnr.it

F. Kadirov · R. Safarov · G. Babayev
Institute of Geology and Geophysics, ANAS, H.Javid Av., 119, AZ1143 Baku, Azerbaijan

G. Yetirmishli · S. Ismaylova
Republican Seismological Survey Center of ANAS, Nigar Rafibeyli str., 25, AZ1001 Baku, Azerbaijan

is caused by intensive geodynamic interaction of the Eurasian and Arabian lithospheric plates (McKenzie 1972; Reilinger et al. 2006; Kadirov et al. 2012; Kadirov et al. 2015).

Although the territory of Azerbaijan represents one of the most seismically active regions worldwide, and in the past several strong and catastrophic earthquakes with magnitude $M \geq 6$ occurred (like the Goygol earthquake (1139), the Ganja earthquake (1235), the Eastern Caucasian earthquake (1668), the Mashtaga earthquake (1842), and the numerous Shamakhi earthquakes (1192, 1667, 1669, 1828, 1859, 1868, 1872, 1902), or Caspian earthquakes (957, 1812, 1842, 1852, 1911, 1935, 1961, 1963, 1986, 1989, 2000) that triggered earth relief changing, destroyed buildings completely and caused numerous casualties, it was only after the earthquake in the Caspian Sea occurred on November 25, 2000 ($M = 6.3$; $\varphi = 40°$, $\lambda = 50°$, $h = 35$ km) that the seismic monitoring of Azerbaijan was improved by the installation of modern telemetric stations with satellite communications system (Yetirmishli et al. 2013; Kadirov et al. 2013) providing a rather good spatial coverage of the whole territory and surrounding regions.

In the territory of Azerbaijan, there are also numerous mud volcanoes which are perhaps under the influence of the crust deformations and earthquakes (Fig. 1). The number of mud volcanoes located on land and at sea exceeds 250. Many mud volcanoes are active at the present time (Yakubov et al. 1971; Aliyev et al. 2009, 2015). A relationship between the occurrence of large earthquakes and the eruptions of close mud volcanoes is well known and it is studied in works (Mellors et al.
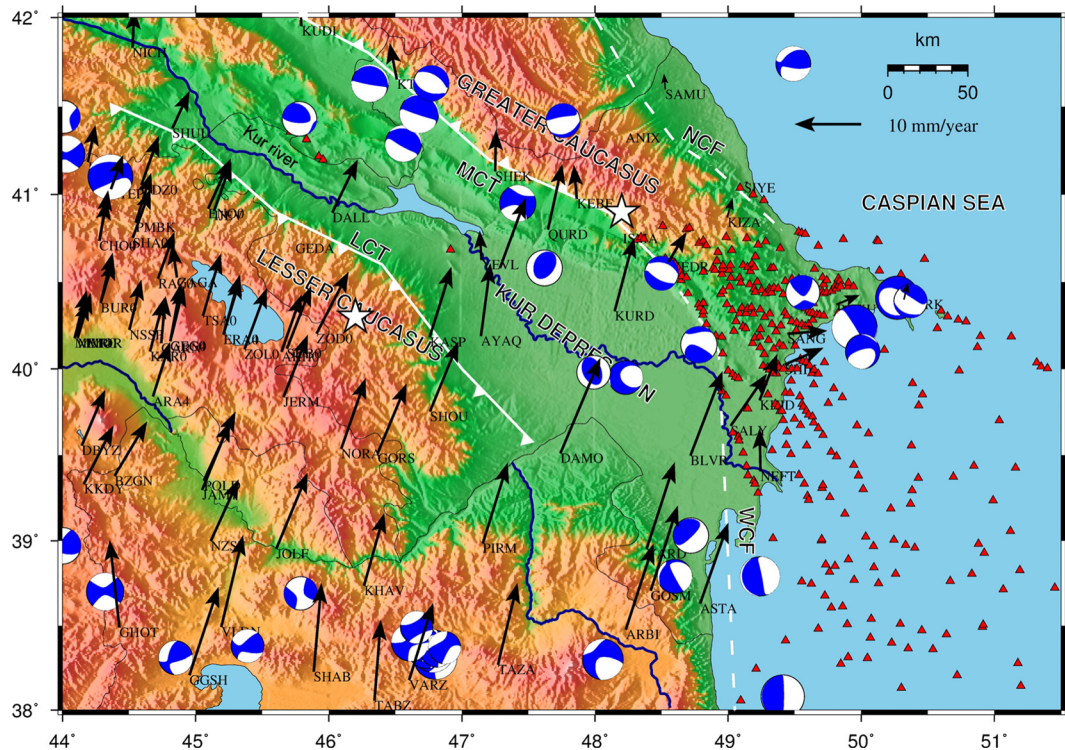
🖄 Springer

Fig. 1 Overview of the tectonics of the Azerbaijan. *Black vectors* are GPS velocities relative to Eurasia from Reilinger et al. (2006). *Red triangles* are mud volcanoes. The focal mechanism solutions are from Global CMT catalog (Ekström and Nettles 1997; Huang et al. 1997; Chen et al. 2001) and the *white star* marks the approximate location of the 1902 Shamakhi and 1139 Ganja earthquakes. *NCT* North Caucasus Thrust fault, *MCT* Main Caucasus Thrust fault, *LCT* Lesser Caucasus Thrust fault, *WCF* West Caspian fault, *NCF* North Caspian fault. The figure was generated using the Generic Mapping Tools (GMT) software (Wessel et al. 2013)

2007; Babayev et al. 2014). Mellors et al. (2007) showed that there is a statistically significant number of mud eruptions triggered by earthquakes by analyzing their temporal–spatial relationships especially in Azerbaijan. Babayev et al. investigated the evaluation of both the static and dynamic strains induced by earthquakes in the substratum of mud volcanoes. A relationship between the occurrence of the crust deformations (GPS velocity) and the activity of mud volcanoes is studied in works (Kadirov et al. 2014; Kadirov and Safarov 2013). The analysis of the relationships between the contemporary deformation processes and mud volcanic activity overall demonstrates the predominance of vertical displacements, which may result from the horizontal compression, where horizontal strains act as triggers.

With the exception of some case studies, mainly focused on seismic hazards and risk of some regions within the Azerbaijani territory (Babayev 2010; Babayev and Telesca 2014), an exhaustive statistical analysis of the properties of the space-time-magnitude

distribution of the entire instrumental seismic catalog of Azerbaijan is still lacking, up to our knowledge.

Therefore, the aim of the present study is to furnish a detailed picture of the statistical properties of the most updated seismic catalog of Azerbaijan and surrounding regions from 2003 to 2016.

2 Seismo-tectonic settings

The territory of Azerbaijan represents the mountainous section of the Greater Caucasus, the Lesser Caucasus, Kur depression zone, and the South Caspian Basin (Fig. 1). Mountains of the Greater and Lesser Caucasus extend between the Black and Caspian seas and creates a part of the continuous Alpine-Himalayan orogenic belt (Nemčok et al. 2011; Kadirov et al. 2012; Alizadeh et al. 2016) (Fig. 1). Greater and Lesser Caucasus is the main orogens of the Azerbaijan earthquake-prone country. The Azerbaijan territory has been exposed to the

continuous collision between Arabian and Eurasian plates (Mckenzie 1972; Sengor et al. 1985; Jackson 1992; Philip et al. 2003; Reilinger et al. 2006; Kadirov et al. 2012; Kadirov et al. 2015; Alizadeh et al. 2016). The collision closed the Greater Caucasus region, further deformed it together with the Eurasian Platform during Middle-Late Miocene, and the Kur Basin and the Greater Caucasus become zones of the maximum underthrusting (Nemčok et al. 2011).

Plate tectonic reconstructions provide only broad constraints on the timing of the initial collision of the Arabian Plate with Eurasia of between 10 and 30 Ma BP (e.g., Allen et al. 2004; Kadirov et al. 2008; Alizadeh et al. 2016) and indicate that the rate of northward motion of Arabia relative to Eurasia has remained more or less constant at about 20 mm/year since collision began (Reilinger et al. 2006). These reconstructions imply that Arabia has progressed from 200 to 600 km "into" space formerly occupied by Eurasian continental lithosphere. This "intrusion" of Arabia into Eurasia continues to be accommodated by lithospheric shortening on roughly E-W striking thrust faults and lateral displacement of lithosphere out of the collision zone along right-lateral strike-slip faults (McKenzie 1972; Sengor et al. 1985; Jackson 1992; Reilinger et al. 2006). These regional tectonic processes give rise to earthquakes that have devastated the Caucasus region throughout recorded history.

Repeating GPS measurements in Azerbaijan during the period 1998–2016 were providing direct observations of present-day surface motions (Fig. 1). They clearly define active convergence between the Lesser Caucasus/Kur depression and the Greater Caucasus with strain concentrated along MCT (Philip et al. 2003; Reilinger et al. 2006; Kadirov et al. 2008; Kadirov et al. 2012; Telesca et al. 2015). Present-day slip rates on the MCT decrease from 10 ± 1 mm/year in eastern Azerbaijan to 4 ± 1 mm/year in western Azerbaijan (Kadirov et al. 2008; Kadirov et al. 2015). In the Lesser and Greater Caucasus, the observed stress pattern shows lateral variations. The seismic activity pattern provides important information about the recent block differentiation.

The predominant faults in Azerbaijan are longitudinal sublatitudinal of the Caucasus extension which considerably obscures the appearance of the transversal faults. Tectonics of Azerbaijan is characterized by main fault structures which are North Caucasus Thrust fault (NCT),

Main Caucasus Thrust fault (MCT), Lesser Caucasus Thrust fault (LCT), West Caspian fault (WCF), North Caspian fault (NCF) (Fig. 1). The compression is observed in the western part of Azerbaijan through MCT fault and the depression occurs southward alongside the northern edge of the mountain ring. Besides, an obvious transition from the left-lateral strike-slip to the mostly right-lateral strike-slip occurs towards southern part of the Greater Caucasus Mountain Range. Reverse dip slips in the north-north-eastern direction are predominant along MCT, which results in the crustal contraction along MCT (Nemčok et al. 2011; Kadirov 2000; Babayev and Telesca 2014; Telesca et al. 2013; Kadirov et al. 2015; Alizadeh et al. 2016). Figure 1 shows faults determined by surface geological mapping and those interpreted from earthquake and gravity data. This set of faults demonstrates that the majority is formed by NW-SE striking faults. Mapped faults (Alizadeh 2008; Shikhalibeyli 1996; Kadirov 2000), based on observation of the dip-slip displacement component, indicate that some NW-SE striking faults comprise reverse and normal faults (Kadirov 2000; Agayeva and Babayev 2009). Their dip towards NE is prevalent. Mapped NNW-SSE to NE-SW faults in the Greater Caucasus region indicate that they formed as dextral and sinistral strike-slip faults accommodating in homogeneous shortening (Alizadeh 2008; Shikhalibeyli 1996).

Taking into account the geological structure, level of seismicity, complex analysis of GPS velocities (Reilinger et al. 2006), seismicity (Kondorskaya and Shebalin 1982; Gasanov 2003; Babayev 2010; Babayev et al. 2010), fractal dimension of the earthquakes, and the stress state of the Earth's crust (Agayeva and Babayev 2009), Azerbaijan territory can be divided into the several individual large zones: southern slope of the eastern part of Greater Caucasus (SSGC), Kur depression (KD), northern slope of Lesser Caucasus (NSLC), Gusar-Shabran depression (G-SD), Absheron Peninsula (AP), Talish Zone (TZ), and Caspian Sea. There are four seismogenic zones throughout the southern slope of the eastern part of the Greater Caucasus: Balaken-Zagatala, Sheki-Gabala, Shamakhi-Ismayilli and Absheron (Kadirov et al. 2013) (Fig. 2). The Balaken-Zagatala zone and the Shamakhi-Ismayilli zone are characterized by the extension, and the displacements over those areas are mainly normal dip slips and normal dip slips with strike-slip motion. The Sheki-Gabala and the Absheron zones are mostly compression

Fig. 2 The seismogenic zones throughout the southern slope of the eastern part of the Greater Caucasus: *I*—Balaken-Zagatala, *II*—Sheki-Gabala, *III*—Shamakhy-Ismailly, and *IV*—Absheron
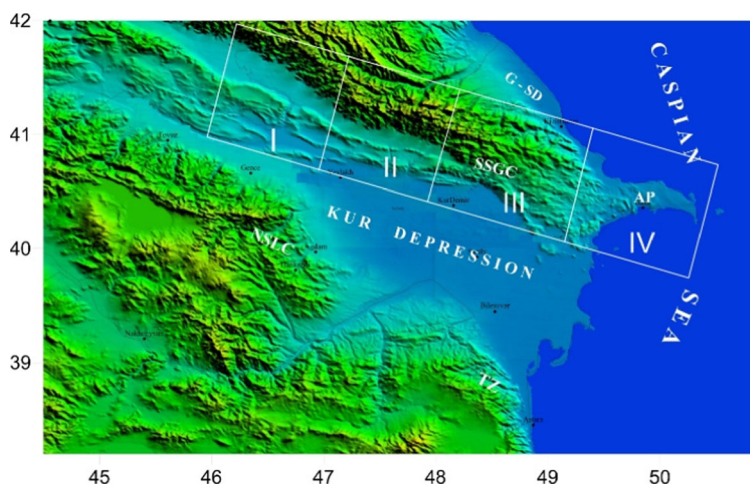
with the thrust and reverse faults (Kadirov et al. 2013). The Lesser Caucasus is characterized by strike-slip fault type, while Talysh Mountains are characterized by thrust regimes.

According to the map of the focal mechanisms and stress distribution (Fig. 1), the thrust fault of horizontal compression trending north-north-east in the western part of the southern Caucasus and east-northeast within the eastern part of the Greater Caucasus occurs (Agayeva and Babayev 2009; Kadirov et al. 2013). The map of focal mechanisms of earthquakes with magnitudes larger than 5 is shown in Fig. 1.

3 Data

Our multiparametric statistical analysis of the seismicity relied on the catalog the Republican Seismic Survey Center of the Azerbaijan National Academy of Sciences of the earthquakes with local magnitude $M \geq 2$, available at the following link: http://www.seismology. az/en/earthquakes#.WMVMgDieaPg (Fig. 3 shows the seismic network of Republican Seismic Survey Center of Azerbaijan National Academy of Sciences). Figure 4 shows the spatial distribution of the investigated seismic catalog from 2003 to 2016.

4 Methods and results

In this study, we investigate the seismicity occurred from January 1, 2003, to April 21, 2016, in the territory of Azerbaijan and surrounding regions by employing

several and independent statistical approaches. Our aim is to get the most exhaustive description of the earthquake process involving the territory of Azerbaijan, by furnishing a complete space-time dynamical characterization of the Azerbaijani seismicity that, up to our knowledge, has not been performed so far.

4.1 The frequency-magnitude distribution

The frequency-magnitude distribution (FMD) in tectonic areas can be fit by the Gutenberg-Richter (GR) law (Gutenberg and Richter 1944) that is a power-law relationship between a threshold magnitude M_{th} and the cumulative number of seismic events with magnitude larger than such a threshold; it is generally expressed as $\log_{10}(N) = a - bM_{th}$ (a line in semi-log scales) where N represents the cumulative number of events whose magnitude is above the threshold, a represents the earthquake productivity, and b is a critical parameter informing about the size distribution of earthquakes (Gutenberg and Richter 1944; Ishimoto and Iida 1939). A large/small b value suggests a relatively larger/smaller proportion of less intense events in relation with the more intense ones. In particular, the b value can indirectly quantify stress crustal conditions (Scholz 1968; Wyss 1973) or identify volumes of active magma bodies (Wiemer et al. 1998). It is even employed to discriminate purely tectonic seismicity ($b < 1.5$–1) from volcano-tectonic earthquakes ($b > 1.5$) that are principally caused by hydraulic fracturing of the host rock induced by overpressurized magma and/or associated fluids. Variations in seismic b value of acoustic emission events during the stress buildup and release on

Fig. 3 The Seismic network of Republican Seismic Survey Center of Azerbaijan National Academy of Sciences

laboratory-created fault zones were investigated (Goebel et al. 2013), and evidence was shown that the *b* value in the size distribution of acoustic emission events decreases linearly with differential stress (Scholz 2015). Tormann et al. (2015) found that *b* changes in space mirroring the tectonic regime. Spada et al. (2013) found a negative correlation between *b*

value and differential stress, confirming, thus, the idea of *b* as stress meters in the Earth's crust (Schorlemmer et al. 2005).

The reliable estimation of *b* for seismicity represents an important task aimed at the characterization of different stages of seismicity evolution and, thus, changes in the dynamic processes; it has also a great

Fig. 4 Spatial distribution of seismicity in Azerbaijan and surrounding regions from 2003 to 2016. The sizes of the *crosses* are proportional to the magnitude of the events
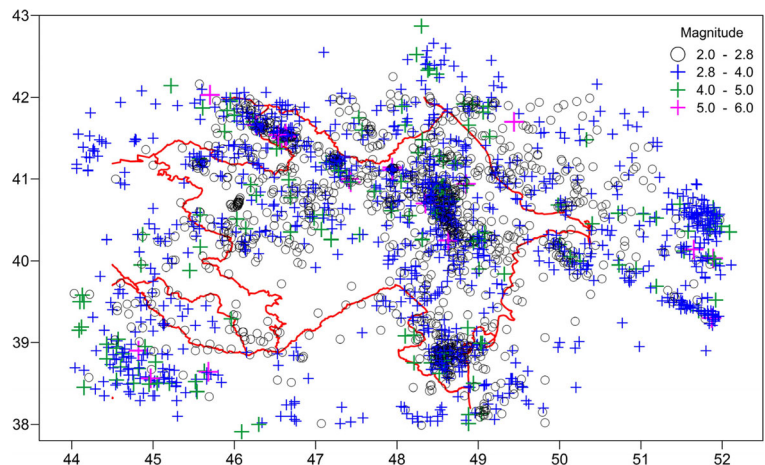
importance in seismic hazard assessments (Naylor et al. 2009).

In our paper, we estimate the b value by means of maximum likelihood method (Aki 1965),

$$b = \frac{\log_{10}(e)}{<M> - \left(M_c - \frac{\Delta M_{bin}}{2}\right)}, \quad (1)$$

where $<M>$ is the mean magnitude of the subset of seismic events with magnitude larger or equal to the completeness magnitude M_c and ΔM_{bin} represents the binning width of the catalog (Utsu 1999).

The standard deviation of the estimate of b is calculated by using the Shi and Bolt's (1982) formula,

$$\sigma_b = 2.3 b^2 \sqrt{\frac{\sum_{i=1}^{N} (M_i - <M>)^2}{N(N-1)}}. \quad (2)$$

The estimation of the b value depends on the estimate of the completeness magnitude M_c which represents the minimum magnitude above which the seismic catalog can be considered complete. Selecting only the earthquakes with magnitude $M \geq M_c$ ensures that the results of the statistical analysis are reliable.

Figure 5 shows the cumulative (CFMD) (squares) and non-cumulative frequency-magnitude distribution (NCFMD) (triangles) of the Azerbaijani seismicity. The CFMD and NCFMD are used to evaluate the completeness magnitude M_c. There are several methods that perform such estimation. Wiemer and Wyss (2000) proposed the method of the maximum curvature (MAXC), which allows a simple estimate of M_c as that magnitude corresponding to the highest frequency of earthquakes in the NCFMD (Fig. 5a). Another method, so called entire magnitude range (EMR) (Woessner and Wiemer 2005) considers the entire magnitude set, whose complete part is modeled by a power-law with a and b value estimated by the MLE method, and the incomplete part is modeled by a normal cumulative distribution function describing the detection capability as a function of magnitude is fitted to the data and depends on μ (magnitude at which 50% of the earthquakes are detected), σ (the standard deviation describing the width of the range where earthquakes are partially detected) and M_c, which represents the lower limit of magnitudes that are detected with probability 1. The M_c corresponds to the magnitude that maximizes the log-likelihood function of a, b, μ, and σ

(Fig. 5b). Wiemer and Wyss (2000) proposed also a method based on the goodness-of-fit (GFT) calculated as the absolute difference of the number of earthquakes in the magnitude bins between the observed CFMD and synthetic CFMDs computed using the a and b values of GR law of the observed dataset for $M \geq M_{th}$ as a function of increasing threshold magnitudes M_{th}. It is taken as M_c of the catalog the magnitude above which the 90% of the observed data are well modeled by a straight line (Fig. 5c). All these methods were implemented in the freely available software package ZMAP (Wiemer 2001). In our case, the three methods furnish different values of M_c: 2.1 (MAXC), 2.5 (EMR), and 2.9 (GFT), and correspondingly different values for the couple (a, b): (4.45, 0.507) (MAXC), (4.68, 0.579) (EMR) and (5.3, 0.763) (GFT). The standard deviation σ_b, calculated by using Eq. (2) are: 0.008 (MAXC), 0.01 (EMR), and 0.02 (GFT). Actually, the shape of NCFMD seems quite unusual, because appears bimodal with the presence of two very close maxima, one at 2.1 and one at 3.0, although the absolute maximum is at 2.1, as identified by the MAXC method. The bimodal shape of the NCFMD leads to clearly lower estimation performance of MAXC and EMR methods; in fact, the GR power-law (red line) does not fit adequately the NCFMD for magnitude larger than M_c, especially at higher ranges. The bimodal shape of the NCFMD is very probably due to a mixing of seismic data recorded by different seismic network spatial configurations: the maximum at 3.1 could be associated to a regional network and the maximum at 2.1 can be associated to a local network. Mignan (2012) found the same phenomenon in the Nevada earthquake catalog whose NCFMD displayed two different maxima due to the superposition of two different NCFMD arising from a regional and local seismic network. Also Wiemer and Wyss (2002) examined several cases of bimodal NCFMDs due, for instance, to contamination by explosions, or to onset of volcano-related events.

In our case, therefore, for the Azerbaijani seismic catalog, there should exist a spatial heterogeneity in M_c that significantly alters the shape of the NCFMD. The estimation of the M_c by using the GFT method, thus, seems more reliable.

Figure 5d shows the variation of b value with the magnitude threshold 2.0 until 4.5, with error bars calculated by using formula (2). It is visible that for thresholds until 2.9 the b value increases with the threshold but it is quite stable for $3.0 \leq$ threshold ≤ 3.8

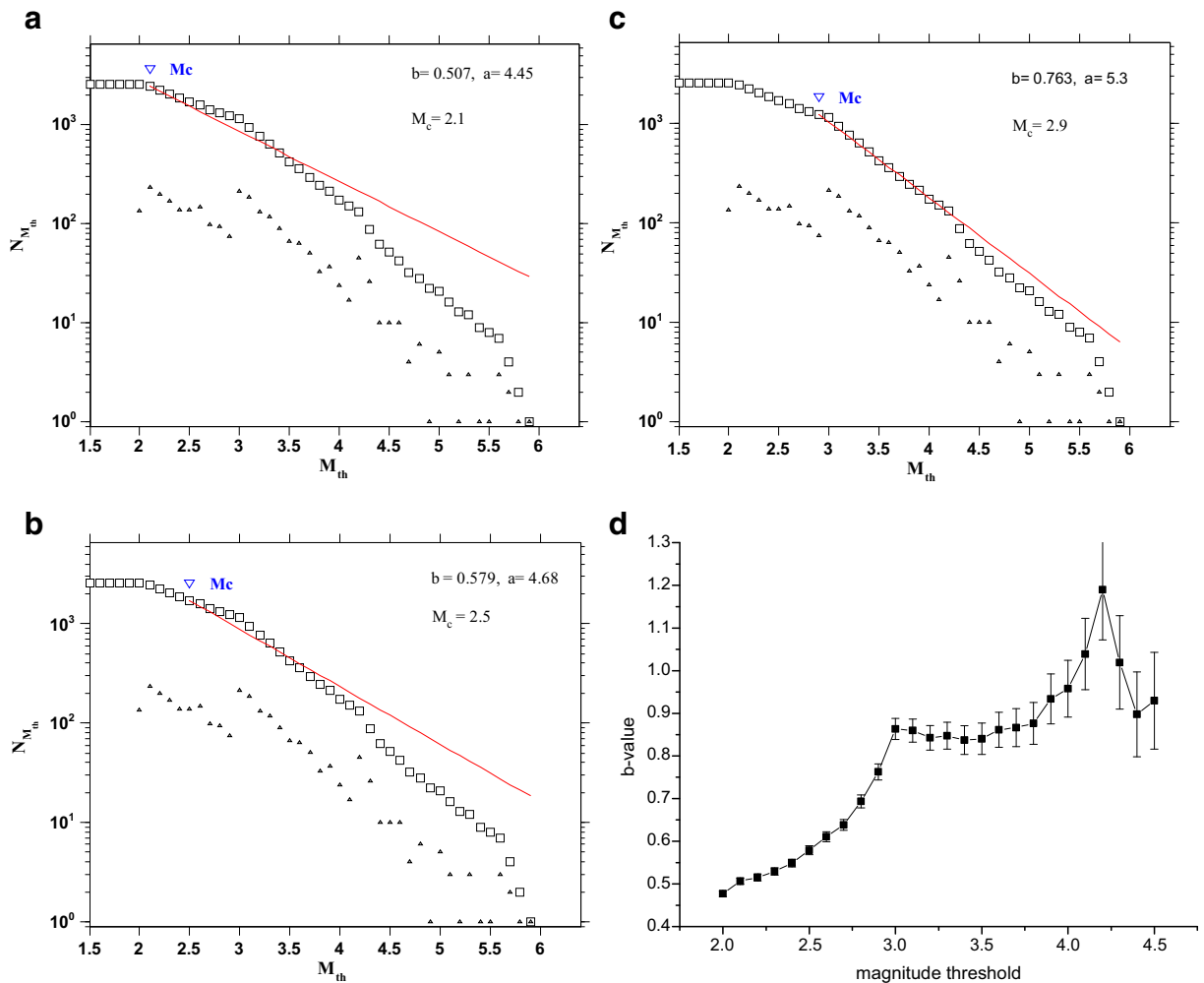**a**

b

c

d

Fig. 5 NCFMD (*triangles*) and CFMD (*squares*) of the Azerbaijani catalog and estimation of the completeness magnitude by using the MAXC (**a**), EMR (**b**), and GFT (**c**) methods. The *red*

line represents the GR law with *a* and *b* value estimated on the base of the value of the completeness magnitude M_c. **d** *b* value versus magnitude threshold

with *b* value around 0.85; for thresholds larger than 3.8, the *b* value peaks at 4.2 but stabilizes again around 0.85 at largest thresholds.

Thus, on the base of all these results, we can assert that the completeness magnitude of the Azerbaijani catalog during the period 2003–2016 is 3.0 and the *b* value of the GR law is about 0.85.

In the next statistical analyses, then, we will consider the subset of seismic events with magnitude $M \geq 3.0$. The number of events with $M \geq 3.0$ is 1163. The spatial distribution of the events is shown in Fig. 4. Figure 6 shows the time-magnitude plot (Fig. 6a) and the time-depth plot (Fig. 6b) for the events with $M \geq 3.0$.

4.2 The coefficient of variation

The coefficient of variation C_v is a simple quantity used to investigate the properties of the temporal distribution of a seismic series. It is defined as

$$C_v = \frac{\sigma}{\mu}, \qquad (3)$$

where σ and μ are the standard deviation and the average of the interevent times (Fig. 7), respectively. If C_v is smaller, equal or higher than 1, the seismic series is regular (or periodic), purely random (or Poissonian) or clustered (Kagan and Jackson
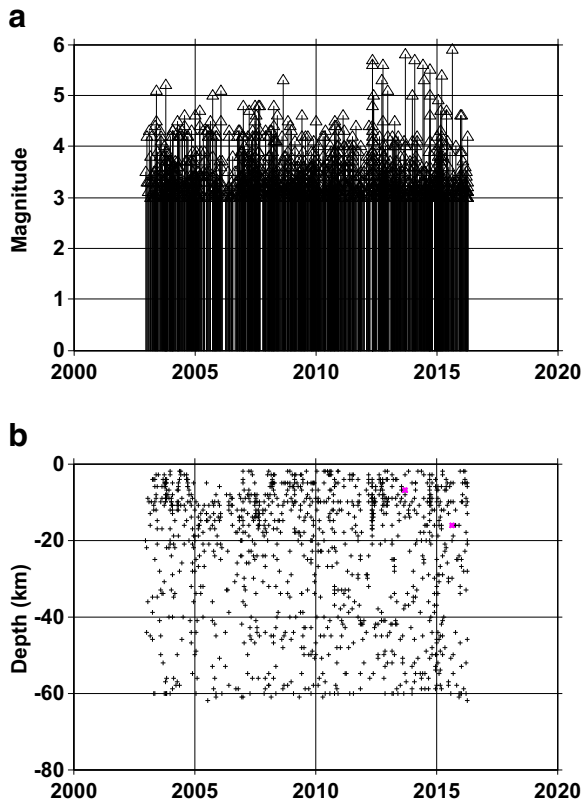
a

b

Fig. 6 a Time-magnitude plot and **b** time-depth plot of the seismicity of the investigated area ($M \geq 2.9$) (the plots were produced by ZMAP software)

1991). The coefficient of variation was extensively employed to identify the type of temporal distribution of earthquakes in many seismic zones worldwide. Recently, Telesca et al. (2016) introduced the local coefficient of variation L_v, defined by

Shinomoto et al. (2005), to analyze the volcano-related seismicity at El Hierro, Canary Islands (Spain):

$$L_v = \frac{1}{N-1} \sum_{i=1}^{N-1} 3 \frac{(T_i - T_{i+1})^2}{(T_i + T_{i+1})^2} \qquad (4)$$

The value of C_v and L_v is 1 for a Poisson process (with exponential probability density function of the interevent times) and is 0 for a periodic process. C_v is able to identify global variability of a whole interevent sequence and can be affected by event rate fluctuation, while L_v identifies local stepwise variability of interevent times, because it is rather independent of slow variation in average rate. Just as an example, if one joins two periodic point processes like those in Fig. 8, $C_v \gg 1$ because globally the process appears highly clustered, but $L_v \sim 0$, due to the regular character of the process at a local scale.

We calculated both the global and the local coefficient variation for the seismicity of Azerbaijan for the earthquakes with magnitude $M \geq 3.0$, and obtained $C_v \sim 1.25$ and $L_v \sim 1.28$. We compared these values with those obtained from 10,000 Poisson processes randomly generated with the same size ($N = 1163$) and mean ($<T> \sim 4.18$ days) as the original seismic interevent time series. The 95% confidence interval, which is given by the 2.5th and 97.5th percentiles of the distribution of C_v and L_v of the Poissonian surrogates, are [0.9448, 1.0579] for C_v and [0.9393, 1.0630] for L_v; and this indicates that both globally and locally, the distribution of the Azerbaijani earthquake occurrence times is clusterized.
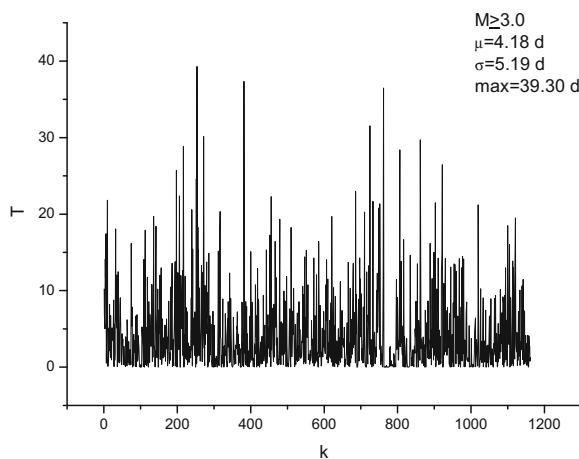

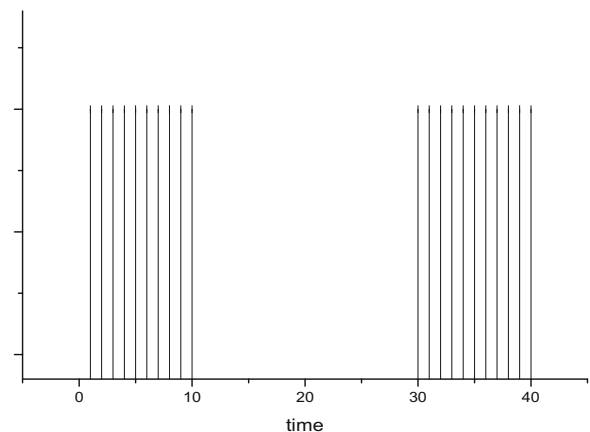**Fig. 7** Interevent time series of the Azerbaijani seismic catalog

Fig. 8 Example of superposition of two periodic finite point processes

4.3 The scaling exponent of the magnitude time series

The Detrended Fluctuation Analysis (DFA) (Peng et al. 1994) is a well-known method employed to detect long-range correlations in non-stationary series; it was used in many scientific fields (Telesca and Lovallo 2009; Telesca and Lovallo 2010; Telesca and Lovallo 2011; Telesca et al. 2012). Telesca et al. (2016) found a relationship between the enhancement of the scaling exponent calculated by the DFA (see later in the text) during the reactivation periods of the volcanic activity at El Hierro, Canary Islands (Spain) in the 2011–2014. Varotsos et al. (2014) applied the DFA to the series of magnitude of earthquakes occurred in different seismo-tectonic zones worldwide and found characteristic variations in the temporal correlations between earthquake magnitudes and interpreted such variations in terms of earthquake prediction. Lennartz et al. (2008) analyzed by using the DFA the long-range correlations of the magnitude series of earthquakes occurred in Northern and Southern California and evidenced that the temporal fluctuations of magnitudes are characterized by long-term memory in the seismicity. Varotsos et al. (2012) found that in stationary regimes, California seismic activity is characterized by long-range temporal correlations among magnitudes (indicated by a DFA scaling exponent ~0.6), while before the occurrence of large shocks, these correlations break down.

From all above, we can argue that the analysis of long-range correlations in earthquake magnitude series can allow gaining insight into the dynamics of a seismic process.

The DFA method is described below:

i) The magnitude series M_i, where $i = 1,\ldots,N$, and N is the total number of events is integrated

$$y_k = \sum_{i=1}^{k} M_i - < M >,\qquad(5)$$

where $<M>$ is the average magnitude of the sequence;

ii) The integrated series y_k is divided into windows of same length n;

for each n-size window, the least square line $y_{n,k}$ fits y_k and is subtracted from y_k;

iii) The fluctuation, F_n, is calculated

$$F_n = \sqrt{\frac{1}{N}\sum_{k=1}^{N}\left[y_k - y_{n,k}\right]^2};\qquad(6)$$

iv) The steps i–iv are repeated for all the available window sizes n; if the relationship between $F_n \sim n$ is a power-law, the magnitudes are long-range correlated:

$$F_n \sim n^{\alpha};\qquad(7)$$

v) From the numerical value of the scaling exponent α, we can get information about the type of correlations: if the magnitude is uncorrelated, then $\alpha = 0.5$; if the magnitudes are persistently correlated (meaning that a large (small) magnitude (compared to the mean) has larger probability to be followed by a large (small) magnitude), then $\alpha > 0.5$; if the magnitudes are antipersistently correlated (meaning that a large (small) magnitude (compared to the mean) has larger probability to be followed by a small (large) magnitude), then $\alpha < 0.5$.

Figure 9 shows the fluctuation function F_n of the magnitude series ($M \geq 3.0$) of the Azerbaijani catalog plotted in log-log scales. The fluctuation function displays a very clear power-law behavior (indicated by the linear shape in bilogarithmic scales). The slope of the
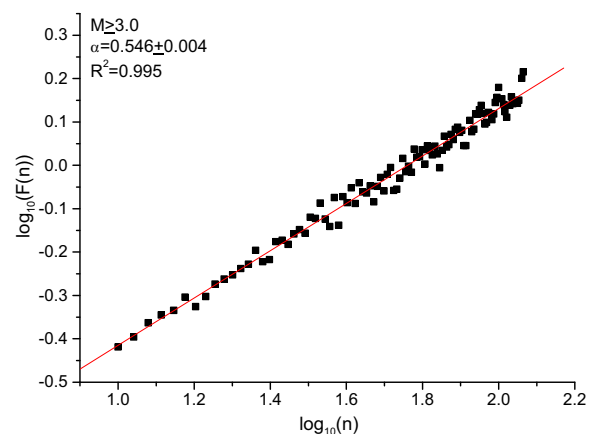

Fig. 9 Log-log plot of the fluctuation function of the magnitude series ($M \geq 3.0$) for the Azerbaijani catalog. The 95% confidence interval on the base of 10,000 surrogates is [0.41, 0.57]

line fitting in a least square sense the fluctuation functions furnishes an estimate of the scaling exponent, $\alpha \sim 0.53$ that indicates that the magnitudes should not be correlated. This indicates that in the period analyzed and for the area investigated, the magnitude of any event that occurred in a certain time and in a certain location does not depend on the magnitude of past events nor will influence the magnitude of future events. The significance of α is evaluated by using the method of surrogates, uncorrelated magnitude sequences constructed by randomly shuffling the magnitudes of the original series. The DFA is then performed on the surrogates and the scaling exponent α_S of surrogates is computed. After generating a sufficiently large number of surrogates and calculated α_S for each one, the 2.5th and 97.5th percentiles of the distribution of α_S will furnish the 95% confidence band. If α lies within the 95% confidence band, this indicates that the original sequence is significantly uncorrelated, otherwise, it is correlated (persistent if above, or antipersistent if below the confidence band). In our case, on the base of 10,000 random surrogates, the 95% confidence band is given by [0.40, 0.62], thus the magnitude series is uncorrelated.

This finding is not trivial, if compared with analogous results obtained in previous studies. Lippiello et al. (2008), for instance, based the feasibility of earthquake predictions also on the dependence of magnitude of an event from those of past earthquakes. In fact, if temporal and/or spatial clusterization is nowadays accepted by the seismological community, much more debatable is the presence of correlations in the magnitude series. Lippiello et al. (2008) suggested that seismic events occur with enhanced probability close in time, space, and even magnitude to previous earthquakes. Sarlis et al. (2009), using the natural time approach verified that correlations between magnitudes are larger for closer in time earthquakes when the maximum interevent interval varies from half a day to 1 min).

In our case, we found that magnitudes are independent, due to the absence of correlations, and thus they are in principle unpredictable. This last finding represents good information, in any case, in the context of seismic hazard analysis of the area.

This finding supports current short-term earthquake clustering models like ETAS, which draw the magnitudes of future events randomly from a GR distribution.

4.4 The correlation dimension of the spatial distribution of the epicenters

The spatial distribution of the earthquake epicenters was analyzed by using the Grassberger-Procaccia method (Grassberger and Procaccia 1983) that is well known in spatial statistics for its efficiency and low noisiness in estimating the correlation dimension D_c of datasets with even small size (Doxas et al. 2010).

Let $N_{R<r}$ be the number of points separated by a distance R less than r; then, the correlation integral is defined as the fraction of couples of points whose interdistance is less than r:

$$C(r) = \frac{2N_{R<r}}{N(N-1)} \tag{8}$$

For fractal spatial point processes, $C(r) \approx r^{D_c}$. The numerical value of the correlation dimension D_c (that is an estimate of the fractal dimension) reveals spatial patterns of the point process. In bidimensional systems, D_c is between 0 and 2; for $D_c = 0$, all the points are clustered into one; for $D_c = 2$, the points are homogeneously distributed. D_c is given by the slope of the line that fits in its linear (scaling) range by the least squares the correlation integral versus r plotted in bilogarithmic scales.

The estimation of the correlation dimension, however, could be affected by bias due to limited size of the dataset and to the improper choice of the scaling range. In order to check these effects, we applied the Grassberger-Procaccia method to a synthetic spatial monofractal Sierpinsky dataset of 1163 point (as many as the epicenters of the Azerbaijani catalog) generated by using the method of Kamer et al. (2013), whose theoretical fractal dimension is D~1.585 (Fig. 10).

Figure 11 shows the correlation integral of the spatial point process shown in Fig. 10. We can see that the correlation integral is not linear for all the spatial scales, but at large scales (for $r > L_{max}$) tends to deviate from linearity and then to bend down. In order to better determine the value of L_{max}, we calculated the slope (namely the correlation dimension D_c) of the line best fitting the correlation integral curve in a spatial scale range $[L_{min}, L_{max}]$, with L_{min} corresponding with the lowest spatial scale and L_{max} varying until the largest available spatial scale. Figure 12 shows the variation of D_c versus L: the minimum absolute deviation from the
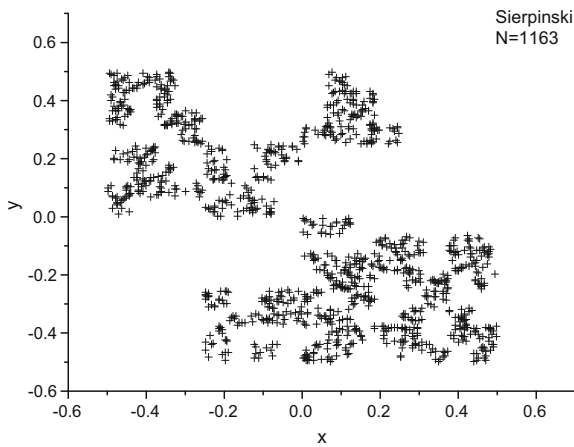
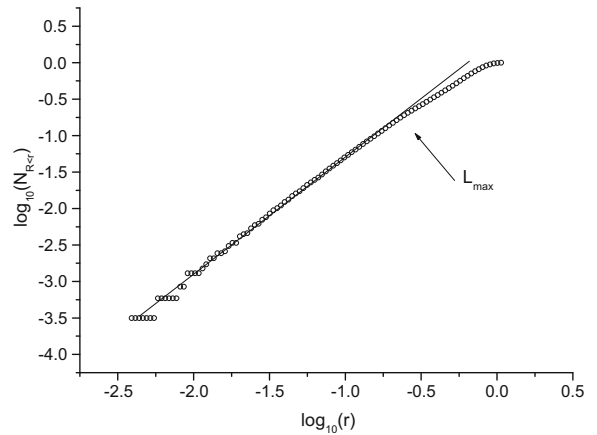**Fig. 10** Random simulation of Sierpinski set

Fig. 11 Correlation integral of the random Sierpinski set shown in Fig. 10

theoretical fractal dimension is for L_{max} = 0.455 that corresponds to ~43% of r_{max}. For this value of L_{max}, the correlation dimension of the Sierpinsky set is 1.584. This result is in agreement with Dongsheng et al. (1994) who found that a value of L_{max} ~20–30% of r_{max} should be enough to avoid finite-size effect visible at large spatial scales (see also Telesca et al. (2001)). Such small absolute value enables us to use the correlation dimension for quantifying the type of spatial distribution of the epicenters of the Azerbaijani seismicity. Figure 13 shows the correlation integral for the Azerbaijani seismicity for spatial scale ranging from ~10^{-1} to ~878 km that is the maximal interevent distance. As it was observed for the synthetic monofractal Sierpinsky set, also here, the relationship between the $\log_{10}(N_{R<r})$ and the spatial scale $\log_{10}(r)$ is not the linear. Analyzing the first derivative (Fig. 14) that is the local slope of the curve, we can see that between L_{min}~10 km and L_{max}~262 km, it is rather constant; within this range, the correlation dimension is D_c~1.38, which indicates that the spatial distribution of epicenters is fractal. Let us notice that the upper value of this range (L_{max}) is about 30% of the maximal interevent distance, in agreement with the results of Dongsheng et al. (1994). The lower value of that range (L_{min}) is about 1% of the maximal interevent distance. Applying the Smith's criterion (Smith 1988)

$$N_{min} \geq \left(\frac{L_{max}}{L_{min}} \frac{2-Q}{2(1-Q)} \right)^{[D]}. \quad (9)$$

where $[D]$ is the integer part of the fractal dimension, $0 \leq Q \leq 1$ is a quality factor, and N_{min} represents the

minimum number required to estimate the fractal dimension, for $[D]$ = 1, Q = 0.95, L_{min} = 10 km and L_{max} = 262 km, $N_{min} \geq 275$; and this criterion is totally satisfied for our dataset.

4.5 Analysis of the temporal variation of the seismic parameters

The analysis of the time variation of the statistical parameters defined in the previous section is important to check if the parameters change with time or are characterized by a rather stable behavior; possible change through time would reveal changes in the dynamics underlying the seismic process. We analyzed the time variation of the statistical seismic parameters by using two approaches: (i) fixed event number (W_N) and (ii) fixed day length (W_D) of a window sweeping the entire catalog with a shift of 1 event or 10 days, respectively. In each window, the completeness magnitude M_c was calculated by the GFT method and only in case the number of events with magnitude $M \geq M_c$ was larger or equal to 50 (in agreement with Woessner and Wiemer (2005)), the statistical seismic parameters were calculated and their value associated with the time of the last event in the window. The minimum number of events per window is enough to significantly calculate the following seismic parameters with a good time resolution: completeness magnitude, b and a values, mean magnitude, C_v and L_v. We did not calculate the time variation of the DFA scaling exponent of the magnitude series and the correlation dimension of the epicenters, since the computation of both these two

Fig. 12 Variation of D_c versus L

$D_c = 1.584$

0.455
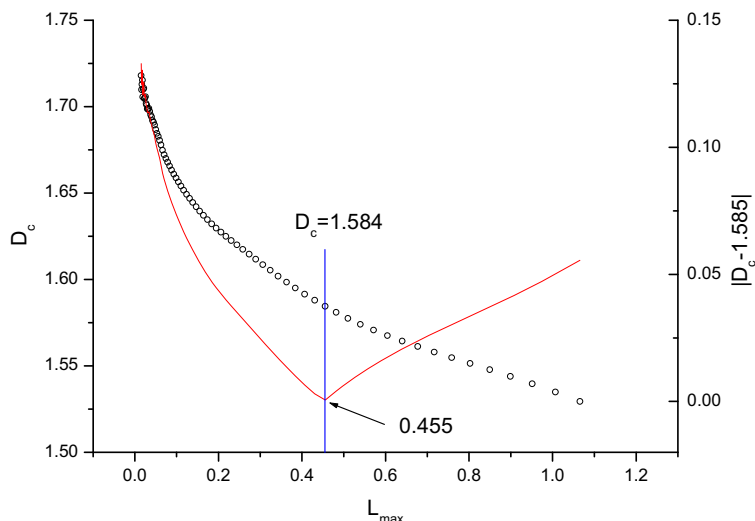
parameters would require a significantly larger window size that would practically impede to perform an analysis of the time variation with a good time resolution.

Figure 15 shows the time variation of the seismic parameters in the case of fixed event number window for two different lengths: $W_N = 100$ (blue circles) and $W_N = 200$ (red circles). In particular, the following parameters were calculated: M_c (Fig. 15a), number of events with magnitude larger or equal to M_c (Fig. 15b), b value (Fig. 15c) (the b value along with its error bar calculated by using formula (2) is shown in Fig. S1), a value (Fig. 15d). Figure 15e, f shows respectively the departure of the C_v and L_v from $C_{v,Pois(97.5\%)}$ and $L_{v,Pois(97.5\%)}$. $C_{v,Pois(97.5\%)}$ (and, analogously, $L_{v,Pois(97.5\%)}$) was calculated in the following manner: (i) for 1000 Poissonian,

sequences were randomly generated with the same length and the same rate as the actual earthquake sequence contained in the moving window; (ii) for each Poissonian sequence, the $C_{v,Pois}$ was computed; (iii) the 97.5% percentile of the distribution of the 1000 values of $C_{v,Pois}$ is calculated; (iv) $C_{v,Pois(97.5\%)}$ represents, then, the superior value of the 95% confidence band of the $C_{v,Pois}$ distribution, meaning that if the value of C_v of the actual earthquake sequence contained in that window is larger than $C_{v,Pois(97.5\%)}$, then the actual earthquake sequence is significantly globally clusterized, otherwise is significantly Poissonian. Figure 16 shows the same seismic parameters as plotted in Fig. 15, but considering a fixed day length window for two different cases: $W_D = 180$ days (blue circles) and $W_D = 365$ days (red circles). We can observe that the time evolution of the seismic parameters is quite
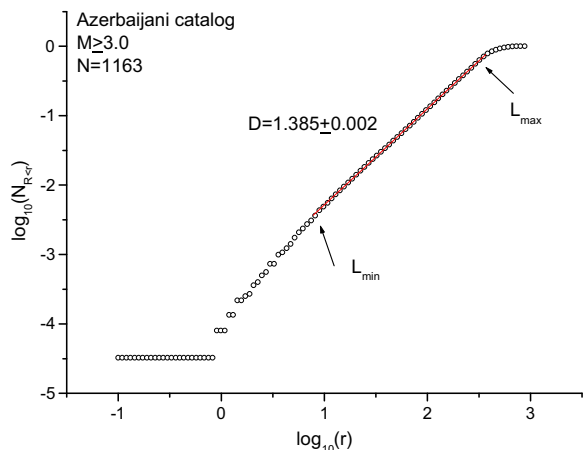

Fig. 13 Correlation integral for the Azerbaijani seismicity for spatial scale ranging from ~10^{-1} to ~878 km
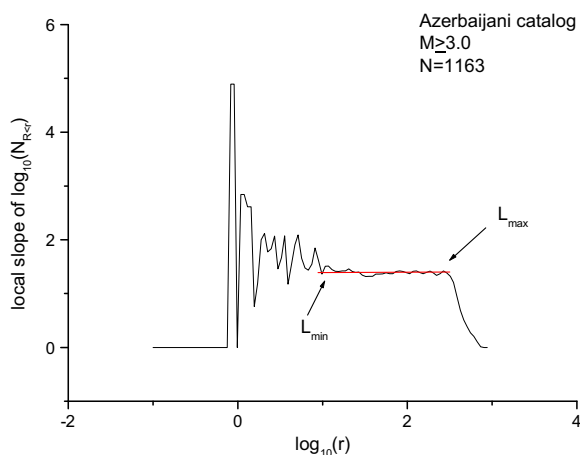

Fig. 14 Local slope of the curve shown in Fig. 13

robust against the type and length of the moving window; they, in fact, show approximately the same behavioral trend in all the cases. The completeness magnitude ranges between 2 and 3.5, being quite stable at 3.0 between 2007 and 2011 (Fig. 15a); during this period, no relatively strong events occurred. Relatively short-range fluctuations in M_c are especially evidenced from 2011 to 2016, indicated by a certain variability of the parameter between 2.0 and 3.5. During the same period, also the number of events with magnitude larger or equal to M_c is quite unstable through time; this is probably due to the occurrence of several relatively strong earthquakes ($M \geq 5$) along with their aftershock sequences and to the mixing of different seismic sources in the same time window. Similar behavior is shown by the other parameters (a value, b value) highly fluctuating between 2011 and 2016. In particular, it is observed a certain relationship between the range of variability of the b value and the occurrence frequency of relatively strong earthquakes (Figs. 15d and 16d): in the period between 2007 and 2011, it ranges between ~0.7 and ~1.25, and between 2011 and 2016, it ranges between ~0.5 and ~1.0. This indicates that in the first period a relatively large number of small events are generated and a low stress characterizing the investigated area; while in the second period, relatively more large earthquakes are generated and a high level of stress is present in the area. On the base of the time variation of C_v-$C_{v,Pois(97.5\%)}$ (Figs. 15g and 16g) and L_v-$L_{v,Pois(97.5\%)}$ (Figs. 15h and 16h), we can see that the peaks of time clusterization both a global and local scale could be associated to the strongest events of the sequence.

4.6 Analysis of the spatial variation of M_c and b value

Since the data is sampled over a large and potentially strongly inhomogeneous area, we performed an analysis of the spatial variability of the completeness magnitude and b value. In fact, the gradient shown in the time variation of b could either mean that the conditions in the same region change, or that no temporal changes exist, but different regions with a different overall b value have been activated. And of course, there might be mixtures. Analogously, M_c depends on network configuration, and unless there have been campaigns during which more stations were used equally over the whole study region, the times of apparently improved M_c of as much as a unit of magnitude, could be associated with periods in which the seismicity concentrated in a region

of better network coverage overall or a local campaign with additional stations. Therefore, in order to check on all these aspects, we superimposed to the investigation territory a spatial grid with square cell side of 0.01° in latitude and longitude. For each node, we considered a circle of 50 km radius and calculated for the earthquakes included within it the number of earthquakes (Fig. 17a), the completeness magnitude M_c (Fig. 17b), the number of events with $M \geq M_c$ (Fig. 17c), and only in case this number if larger or equal to 50 events, the b value is estimated (Fig. 17d). The b value spatial variation can be interpreted in terms of stress changes across collision zone along Main Caucasus Trust (MCT) thrust fault and West Caspian fault (WCF). The decrease of the b value from south to north along the WCF is an indication of higher stress in northern part of the region. It might be reasonable to connect this low b value region with a "harder" patch on the fault. Based on new GPS observations on the Absheron peninsula and along the western coastal side of the Caspian Sea south of Absheron peninsula, it is evidenced that below the 40° E latitude between 48° and 49° longitude, the MCT turns sharply to the south, crossing the Kur depression and extending along the western side of the Caspian Sea. While the MCT is predominantly a thrust fault, the WCF has a substantial right-lateral, strike-slip component, at least in the region immediately south of the Absheron Peninsula. The existence of WCF is also supported by the topographic path of the Kur River, which sharply turns to the south at 40° E latitude. This inflection is partly marked by the region of submeridional discontinuances, generally typical of plastic rocks of depression (Philip et al. 1989; Saintot et al. 2006; Kadirov et al. 2012; Alizadeh et al. 2016). The central part of this strike-slip fault zone (near SALY, BLVR, and NEFT GPS points (see Fig. 1)) is characterized by very low seismicity. However, whether this segment is creeping aseismically or accumulating strain without generating seismicity still remains uncertain (Kadirov et al. 2015).

The low b values (0.60–0.70) in the central part of the southern Talysh seismic zone surrounded by areas of increased values of b (≥ 0.90) evidence the presence of relatively more solid crust material than in Kur depression; here, folded rocks of the Oligocene-Miocene age lie on volcanic rocks of the Eocene age (Alizadeh 2008; Alizadeh et al.2016).

Except western part of the Lesser Caucasus, there is a very low strain accumulation within the Kur basin; in fact, very low b values can be observed along MCT.
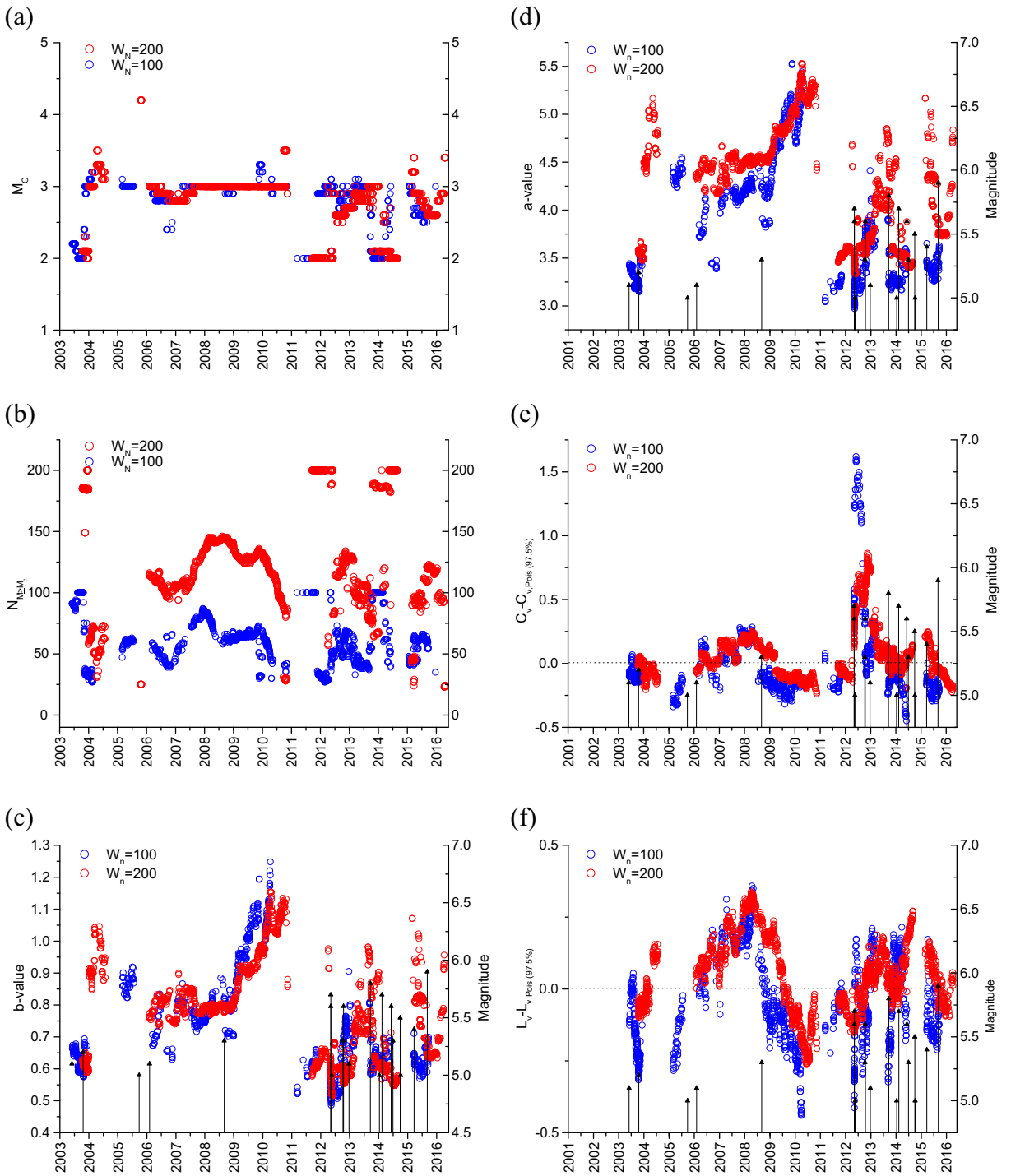
Fig. 15 Time variation of M_c (**a**), number of events with magnitude larger or equal to M_c (**b**), b value (**c**), a value (**d**), departure of the C_v from $C_{v,\text{Pois}(97.5\%)}$ (**e**), and departure of L_v from $L_{v,\text{Pois}(97.5\%)}$ (**f**), in 100 event number window size (*blue*) and 200 event number

window size (*red*). The error on b value was calculated by using Shi and Bolt's formula (1982) are 0.04 and 0.18 ($W_n = 100$) and 0.03 and 0.13 ($W_n = 200$)
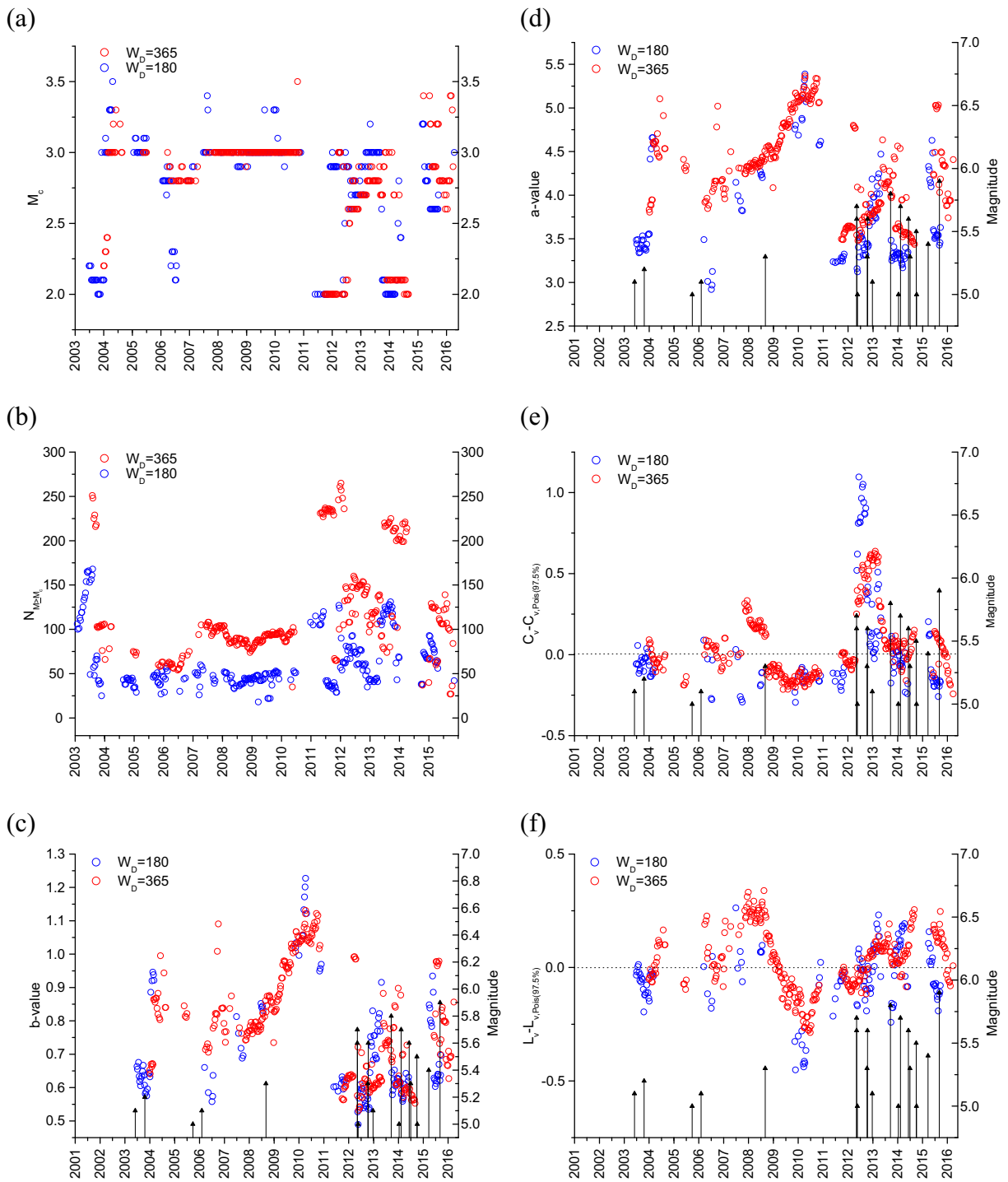
Fig. 16 Time variation of M_c (**a**), number of events with magnitude larger or equal to M_c (**b**), b value (**c**), a value (**d**), departure of the C_v from $C_{v,Pois(97.5\%)}$ (**e**) and departure of L_v from $L_{v,Pois(97.5\%)}$ (**f**), in 180-day window size (*blue*) and 365-day window size (*red*).

The maximum and minimum error on b value calculated by using Shi and Bolt's formula (1982) are 0.04 and 0.17 ($W_D = 180$) and 0.03 and 0.17 ($W_D = 365$)
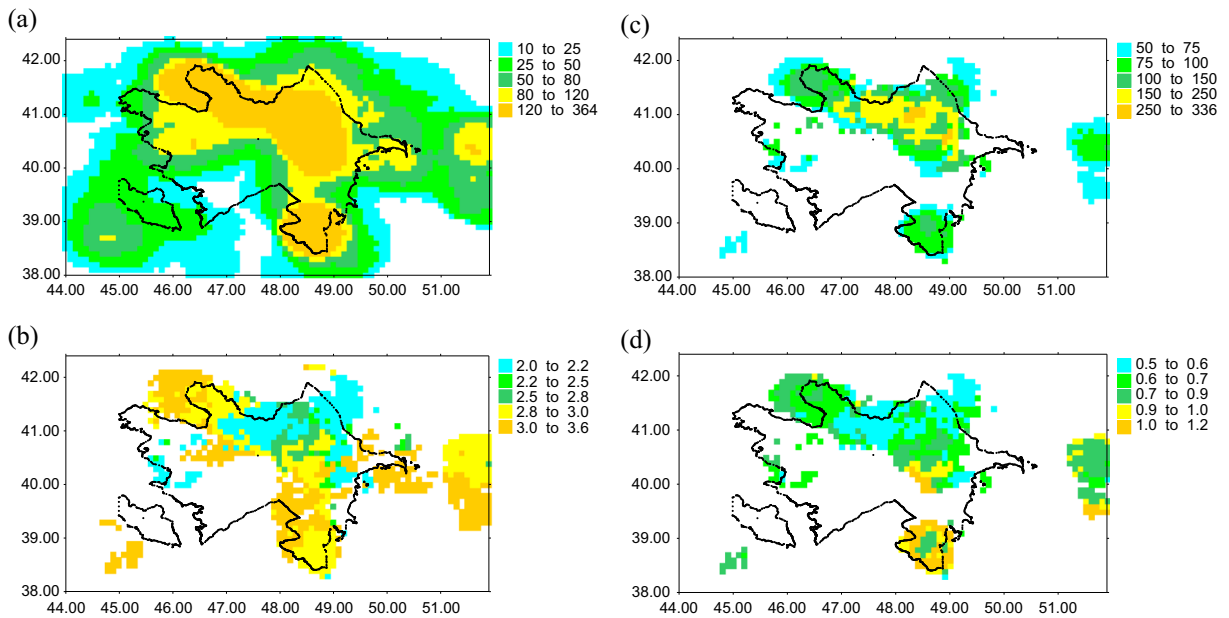
Fig. 17 Spatial distribution of **a** number of events, **b** M_c, **c** number of events with $M \geq M_c$, **d** b value

Particularly, at the central part of the MCT, it becomes minimal, and this is the most seismically active segment. This part of MCT has broken historically in shallow (~15–20 km) continental thrust events including highly destructive earthquakes in 1191, 1859, and 1902 in the Shamakhi region (e.g., Kondorskaya et al. 1977; Triep et al. 1995). It is possible that the differences on seismic regime and estimates of b value at MCT and Kur depression are due to differences in the nature of the crust and lithosphere, which is more soft and thin composed by quaternary marine, marine terrigenous sediments for the Kur Depression and more solid with very thick and consolidated sediments in the MCT and Talysh (Saatli ultradeep well 1999; Allen et al. 2004; Vincent et al. 2005). It is also possible that the different stress regimes trusting along the MCT, strike-slip along the WCF, reflect the different dynamics. Furthermore, the evidence of mud volcanoes distributed to the east of WCF in the eastern Kur depression and in Absheron peninsula can also be the reason of less seismicity (due to more plastic crust material).

5 Conclusions

The present study furnishes a detailed picture of the statistical properties of the spatial, temporal, and magnitude distribution of the 2003–2016 instrumental

seismic catalog of Azerbaijan and surrounding regions that represent one of the most seismically active areas worldwide. The statistical analysis has been performed by using standard and non-standard methodologies to get the most exhaustive description of the catalog. The main findings are as follows:

1) The Gutenberg-Richter law is satisfied for $M \geq 2.9$ with a b value of 0.76, by using the GFT method.

2) The time clustering of the complete catalog was investigated by using the global (C_v) and local (L_v) coefficient of variation, obtaining the values $C_v \sim 1.23$ and $L_v \sim 1.26$ with a 95% confidence interval of [0.9459, 1.0566] and [0.9391, 1.0598], respectively, that indicate time clusterization of the events at both global and local scale.

3) The magnitude series are uncorrelated, and this indicates that they are in principle unpredictable; this finding represents an important information in the context of seismic hazard analysis of the area.

4) The spatial distribution of the epicenters of the Azerbaijani earthquakes is fractal for spatial scales ranging from ~10 to ~262 km.

5) The time variation of the analyzed seismic parameters (M_c, number of events with magnitude larger or equal to M_c, b value, a value, C_v, and L_v) show that from 2011 to 2016, the completeness magnitude is weakly fluctuating, along with the number of

events; other parameters (*a* value, *b* value, <*M*>) show a very visible variation during the same period. The behavior shown by these seismic parameters between 2011 and 2016 could be linked with the occurrence of the strongest events associated with a high level of stress in the area, to which also high time clusterization both a global and local scale could be associated.

6) The spatial variation of the seismic parameters (M_c, number of events with magnitude larger or equal to M_c, *b* value) show a highly space variability connected with the peculiar seismo-tectonic settings of the different areas of Azerbaijan.

References

Agayeva S, Babayev G (2009) Analysis of earthquake focal mechanisms for greater and lesser Caucasus applying the method of World Stress Map, Nafta-Press. Baku 2: 40–44

Aki K (1965) Maximum likelihood estimate of b in the formula log(N)=a-bM and its confidence limits. Bull Earthq Res Inst Tokyo Univ 43:237–239

Aliyev AA, Guliev IS, Rakhmanov RR (2009) Catalog of mud volcanoes eruptions of Azerbaijan (1810–2007). Nafta-Press, Baku, p 105

Aliyev Ad A, Guliev IS, Dadashov FH, Rahmanov RR (2015) Atlas of the world mud volcanoes. Nafta-Press, Baku, p 322

Alizadeh AA (Ed) (2008) Geological map of Azerbaijan Republic, Scale 1:500,000, with Explanatory Notes. Baki Kartoqrafiya Fabriki

Alizadeh AA, Guliyev IS, Kadirov FA, Eppelbaum LV (2016) Geosciences of Azerbaijan. Volume I: geology. 2016. 340 p. Springer International Publishing. doi:10.1007/978-3-319-27395-2.239

Allen M, Jackson J, Walker R (2004) Late Ceno- zoic reorganization of the Arabia-Eurasia collision and the comparison of short-term and long-term deformation rates. Tectonics 23. doi:10.1029/2003TC001530

Babayev G, Tibaldi A, Bonali FL, Kadirov F (2014) Evaluation of earthquake-induced strain in promoting mud eruptions: the case of Shamakhi–Gobustan–Absheron areas. Azerbaijan, Nat Hazards 72:789–808. doi:10.1007/s11069-014-1035-5

Babayev G (2010) About some aspects of probabilistic seismic hazard assessment of Absheron peninsula. Republican Seismic Survey Center of Azerbaijan National Academy of Sciences. Catalogue of Seismoforecasting Research Carried Out in Azerbaijan Territory in 2009, "Teknur", Baku, 59–64 (in Russian)

Babayev G, Ismail-Zadeh A, Le Moüel J-L (2010) Scenario-based earthquake hazard and risk assessment for Baku (Azerbaijan). Nat Hazards Earth Syst Sci 10:2697–2712

Babayev G, Telesca L (2014) Strong motion scenario of 25th November 2000 earthquake for Absheron peninsula (Azerbaijan). Nat Hazards 73:1647–1661

Dongsheng L, Zhaobi Z, Binghong W (1994) Research into the multifractal of earthquake spatial distribution. Tectonophysics 233:91–97

Doxas I, Dennis S, William LO (2010) The dimensionality of discourse. Proc Nat Ac Sci 107:4866–4871

Gasanov A (2003) Earthquakes of Azerbaijan for 1983–2002. Baku, Elm, p 185 (in Russian)

Goebel THW, Schorlemmer D, Becker TW, Dresen G, Sammis CG (2013) Acoustic emissions document stress changes over many seismic cycles in stick-slip experiments. Geophys Res Lett 40:2049–2054

Grassberger P, Procaccia I (1983) Measuring the strangeness of strange attractors. Physica D 9:189–208

Kadirov FA, Guliyev IS, Feyzullayev AA, Safarov RT, Mammadov SK, Babayev GR, Rashidov TM (2014) GPS-based crustal deformations in Azerbaijan and their influence on seismicity and mud volcanism.Izvestiya. Physics of the Solid Earth 50:814–823. doi:10.1134/S1069351314060020

Gutenberg R, Richter CF (1944) Frequency of earthquakes in California. Bull Seism Soc Am 34:185–188

Ishimoto M, Iida K (1939) Observations of earthquakes registered with the microseismograph constructed recently. Bull Earthq Res Inst 17:443–478

Jackson J (1992) Partitioning of strike slip and convergent motion between Eurasia and Arabia in eastern Turkey and the Caucasus. J Geophys Res 97:12471–12479

Kadirov FA (2000) Gravity field and models of deep structure of Azerbaijan. Nafta-Press, Baku, p 112

Kadirov F, Floyd M, Alizadeh A, Guliev I, Reilinger RE, Kuleli S, King R, Toksoz MN (2012) Kinematics of the eastern Caucasus near Baku. Azerbaijan, Natural Hazards 63:997–1006. doi:10.1007/s11069-012-0199-0

Kadirov FA, Floyd M, Reilinger R, Alizadeh A, Guliyev IS, Mammadov SG, Safarov RT. (2015) Active geodynamics of the Caucasus region: implications for earthquake hazards in Azerbaijan. Proceedings of Azerbaijan National Academy of Sciences, The Sciences of Earth, 3, 3–17

Kadirov FA, Gadirov AG, Babayev GR, Agayeva ST, Mammadov SK, Garagezova NR, Safarov RT (2013) Seismic zoning of the southern slope of greater Caucasus from the fractal parameters of the earthquakes, stress state and GPS velocities, Izvestiya, Physics of the solid earth, 49, 554–562 (original in Russian)

Kadirov F, Mammadov S, Reilinger R, McClusky S (2008) Some new data on modern tectonic deformation and active faulting in Azerbaijan (according to Global Positioning System measurements) Proceedings Azerbaijan National Academy of Sciences, Earth's Sciences, 1, 82–88

Kadirov FA, Safarov RT (2013) Deformation of the Earth's crust in Azerbaijan and surroundig territories based on GPS measurements (in Russian), proceedings the Azerbaijan National Academy of Sciences. Sciences of Earth 1:47–55 (in Russian)

Kagan YY, Jackson DD (1991) Long-term earthquake clustering. Geophys J Int 104:117–133

Kamer Y, Ouillon G, Sornette D (2013) Barycentric fixed-mass method for multifractal analysis. Phys Rev E 88:022922

Kondorskaya NV, Shebalin NV (Eds.), (1982) New catalog of strong earthquakes in the USSR from ancient times through 1977, World Data Center for Solid Earth Geophysics, Report SE-31, Boulder, Colorado, pp. 608

Kondorskaya NV, Shebalin NV, Khromenetskaya EA (1977) Novyi katalog sil'nykh zemletryasenii v SSSR s drevnikh vremen do 1975 goda (new catalogue of strong earthquakes in USSR from historical time to 1975). Nauka, Moscow

Lennartz S, Livina VN, Bunde A, Havlin S (2008) Long-term memory in earthquakes and the distribution of interoccurrence times. Europhys Lett 81:69001

Lippiello E, de Arcangelis L, Godano C (2008) Influence of time and space correlations on earthquake magnitude. Phys Rev Lett 100:038501. doi:10.1103/PhysRevLett.100.038501

McKenzie DP (1972) Active tectonics of the Mediterranean region. Geophys J R Asron Soc 30:239–243

Mellors RJ, Kilb D, Aliyev A, Gasanov A, Yetirmishli G (2007) Correlations between earthquakes and large mud volcano eruptions. J Geophys Res 112:B04304. doi:10.1029/2006JB004489

Mignan A (2012) Functional shape of the earthquake frequency-magnitude distribution and completeness magnitude. J Geophys Res 117. doi:10.1029/2012JB009347

Naylor M, Greenhough J, McCloskey J, Bell AF, Main IG (2009) Statistical evaluation of characteristic earthquakes in the frequency magnitude distributions of Sumatra and other subduction zone regions. Geophys Res Lett 36:L20303. doi:10.1029/2009GL040460

Nemčok M, Feyzullayev A, Kadirov A, Zeynalov G, Allen R, Christensen C, Welker B (2011) Neotectonics of the Caucasus and Kura valley, Azerbaijan. Global Engineers & Technologist Review 1:1–14

Peng CK, Buldyrev SV, Havlin S, Simons M, Stanley HE, Goldberger AL (1994) Mosaic organization of DNA nucleotides. Phys Rev E 49:1685–1689

Philip H, Cisternas A, Gvishiani A, Gorshkov A (1989) The Caucasus: an actual example of the initial stages of continental collision. Tectonophysics 161:1–21

Philip H, Cisternas A, Gvishiani A, Gorshkov A (2003) The Caucasus: an actual example of the initial stages of continental collision. Tectonophysics 161:1–21

Reilinger R, McClusky S, Vernant P, Lawrence S, Ergintav S, Cakmak R, Ozener H, Kadirov F, Guliev I, Stepanyan R, Nadariya M, Hahubia G, Mahmoud S, Sakr K, ArRajehi A, Paradissis D, Al-Aydrus A, Prilepin M, Guseva T, Evren E, Dmitrotsa A, Filikov SV, Gomez F, Al-Ghazzi R, Karam G (2006) GPS constraints on continental deformation in the Africa–Arabia–Eurasia continental collision zone and implications for the dynamics of plate interactions. J Geophys Res B5. doi:10.1029/2005JB004051

Saatli ultradeep well (1999) Researches of a deep structure of the Kur intermountain depression on materials of drilling of the Saatli ultradeep well-SG-1. Editors: A.Alizadeh and V.Khain. Baku, "Nafta-Press", 242p

Saintot A, Brunet M-F, Yakovlev F, Sebrier M, Stephenson R, Ershov A, Chalot-Prat F, McCann T (2006) The Mesozoic-Cenozoic tectonic evolution of the Greater Caucasus. In: Gee DG, Stephenson RA (eds) European lithosphere dynamics, vol 32. Geological Society of London Memoir, pp 277–289

Sarlis NV, Skordas ES, Varotsos PA (2009) Multiplicative cascades and seismicity in natural time. Phys Rev E 80:022102

Scholz CH (2015) On the stress dependence of the earthquake b value. Geophys Res Lett 42:1399–1402

Scholz CH (1968) Microfracturing and the inelastic deformation of rock in compression. J Geophys Res 73:1417–1432

Schorlemmer D, Wiemer S, Wyss M (2005) Variations in earthquake-size distribution across different stress regimes. Nature 437:539–542

Sengor AMC, Gorur N, Saroglu F (1985) Strike slip faulting and related basin formation in zones of tectonic escape: Turkey as a case study, in: Strike slip Faulting and Basin Formation. Soc Econ Paleont Min Spec Pub 37:227–264

Shi Y, Bolt BA (1982) The standard error of the magnitude-frequency b-value. Bull Seismol Soc Am 72:1677–1687

Shikhalibeyli E (1996) Some problematic aspects of geological structures and tectonics of Azerbaijan. Baku, "Elm", 48–82. (in Russian)

Shinomoto S, Miura K, Koyama S (2005) A measure of local variation of inter-spike intervals. Biosystems 79:67–72

Smith LA (1988) Intrinsic limits on dimension calculations. Phys Lett A 133:283–288

Spada M, Tormann T, Wiemer S, Enescu B (2013) Generic dependence of the frequency-size distribution of earthquakes on depth and its relation to the strength profile of the crust. Geophys Res Lett 40:709–714

Telesca L, Cuomo V, Lapenna V, Macchiato M (2001) Identifying space-time clustering properties of the 1983-1997 Irpinia-Basilicata (southern Italy) seismicity. Tectonophysics 330:93–102

Telesca L, Lovallo M (2009) Non-uniform scaling features in central Italy seismicity: a non-linear approach in investigating seismic patterns and detection of possible earthquake precursors. Geophys Res Lett 36:L01308

Telesca L, Lovallo M (2010) Long-range dependence in tree-ring width time series of Austrocedrus chilensis revealed by means of the detrended fluctuation analysis. Physica A 389:4096–4104

Telesca L, Lovallo M (2011) Analysis of time dynamics in wind records by means of multifractal detrended fluctuation analysis and Fisher-Shannon information plane. J Stat Mech P07001

Telesca L, Lovallo M, Babayev G, Kadirov F (2013) Spectral and informational analysis of seismicity: an application to the 1996-2012 seismicity of northern Caucasus-Azerbaijan part of Greater Caucasus-Kopet Dag Region. Physica A 392:6064–6078. doi:10.1016/j.physa.2013.07.031

Telesca L, Lovallo M, Lopez C, Martì Molist J (2016) Multiparametric statistical investigation of seismicity occurred at El Hierro (Canary Islands) from 2011 to 2014. Tectonophysics 672-673:121–128

Telesca L, Lovallo M, Mammadov S, Kadirov F, Babayev G (2015) Power spectrum analysis and multifractal detrended fluctuation analysis of Earth's gravity time series. Physica A 428:426–434. doi:10.1016/j.physa.2015.02.034

Telesca L, Pierini JO, Scian B (2012) Investigating the temporal variation of the scaling behavior in rainfall data measured in central Argentina by means of the detrended fluctuation analysis. Physica A 391:1553–1562

Triep EG, Abers GA, Lerner-Lam AL, Mishatkin V, Zakharchenko N, Starovoit O (1995) Active thrust front of

the Greater Caucasus: the April 29, 1991, Racha earthquake sequence and its tectonic implications. J Geophys Res 100. doi:10.1029/94JB02597

Tormann T, Enescu B, Woessner J, Wiemer S (2015) Randomness of megathrust earthquakes implied by rapid stress recovery after the Japan earthquake. Nat Geosci 8:152–158

Utsu T (1999) Representation and analysis of the earthquake size distribution: a historical review and some new approaches. Pageoph 155:509–535

Varotsos PA, Sarlis NV, Skordas ES (2012) Scale-specific order parameter fluctuations of seismicity before mainshocks: natural time and detrended fluctuation analysis. Europhys Lett 99:59001

Varotsos PA, Sarlis NV, Skordas ES (2014) Study of the temporal correlations in the magnitude time series before major earthquakes in Japan. J. Geophys. Res. Space Physics 119:9192–9206

Vincent SJ, Allen MB, Ismail-Zadeh AD, Flecker R, Foland KA, Simmons MD (2005) Insights from the Talysh of Azerbaijan into the Paleogene evolution of the South Caspian region. Bull Geol Soc Am 117:1513–1533

Wessel P, Smith WHF, Scharroo R, Luis JF, Wobbe F (2013) Generic mapping tools: improved version released. EOS Trans AGU 94:409–410

Wiemer S (2001) A software package to analyze seismicity: ZMAP. Seismol Res Lett. doi:10.1785/gssrl.72.3.37

Wiemer S, McNutt SR, Wyss M (1998) Temporal and three-dimensional spatial analysis of the frequency-magnitude distribution near Long Valley Caldera, California. Geophys J Int 134:409–421

Wiemer S, Wyss M (2000) Minimum magnitude of completeness in earthquake catalogs: examples from Alaska, the western United States, and Japan. Bull Seismol Soc Am 90:859–869

Wiemer S, Wyss M (2002) Mapping spatial variability of the frequency-magnitude distribution of earthquakes. Adv Geophys 45:259–302

Woessner J, Wiemer S (2005) Assessing the quality of earthquake catalogues: estimating the magnitude of completeness and its uncertainty. Bull Seismol Soc Am 95:684–698

Wyss M (1973) Towards a physical understanding of the earthquake frequency distribution. Geophys J R Astr Soc 31:341–359

Yakubov AA, Alizade AA, Zeinalov MM, (1971) Mud volcanoes of Azerbajan SSR, atlas. Elm, Baku (in Russian), p. 258

Yetirmishli GJ, Mammadli TY, Kazimova SE, (2013) Features of seismicity of Azerbaijan part of the Greater Caucasus. Journal of Georgian Geophysical Society, Issue (A), Physics of Solid Earth, v. 16a, pp.55–60